ACCSCIENCE PUBLISHING

Explora: Environment and Resource

ORIGINAL RESEARCH ARTICLE

Synergistic GO/MgO nanocomposites with enhanced charge separation for photocatalytic dye degradation

Irfan Toqeer†*, Tahreem Fatima†, Muhammad Afzaal, and Abdul Ghuffar

Department of Physics, Faculty of Engineering and Applied Sciences, Riphah International University, Faisalabad, Punjab, Pakistan

Abstract

The development of efficient and chemically stable photocatalysts with improved charge separation is critical for the remediation of dye-contaminated wastewater. In this study, graphene oxide–magnesium oxide (GO/MgO) nanocomposites with ultralow GO loadings (0–0.05 wt.%) were synthesized through a co-precipitation route and evaluated for ultraviolet (UV)-driven methylene blue (MB) degradation. X-ray diffraction (XRD) results were consistent with the retention of the cubic MgO phase (JCPDS 45-0946) with crystallite refinement from 20.26 to 13.26 nm, while the slight peak-position variations were more consistent with interfacial strain than definitive lattice substitution. UV–visible diffuse reflectance spectra revealed a red shift and bandgap reduction from 5.11 to 4.71 eV. Fourier transform infrared (FTIR) and Raman spectra showed GO-related functional signatures and a decrease in the I_D/I_G ratio (0.886 → 0.830), suggesting strengthened interfacial interactions with increasing GO loading. The optimized 0.05 wt.% GO/MgO sample achieved 91.6% MB degradation within 180 min and exhibited a 5.24-fold enhancement in the apparent pseudo-first-order rate constant (k = 0.00290 min^{-1}) relative to pristine MgO (0.01518 min^{-1}). Photocatalytic efficiency was maximized at pH 7–9 with a catalyst dosage of 0.75 g L^{-1}, and post-reaction XRD/FTIR analysis indicated good structural stability. The enhancement is attributed to crystallite refinement and GO–MgO interfacial charge-transfer pathways inferred from consistent structural/optical–kinetic correlations.

Keywords: Graphene oxide; Magnesium oxide; Nanocomposites; Photocatalysis; Charge separation; Dye degradation

1. Introduction

The escalating discharge of synthetic organic dyes from textile, pharmaceutical, and food processing industries poses severe environmental and health hazards due to their recalcitrant nature and toxic degradation products.[1,2] Methylene blue (MB), a cationic thiazine dye extensively used in textile manufacturing, exhibits high stability and persistence in aquatic ecosystems, necessitating the development of efficient remediation strategies. Among various treatment technologies, heterogeneous photocatalysis has emerged as a promising approach for mineralizing organic pollutants into harmless products, such as CO_2 and H_2O, under ambient conditions.[3]

†*These authors contributed equally to this work.*

***Corresponding author:**
Irfan Toqeer
(irfan.toqeer@riphahfsd.edu.pk)

Citation: Toqeer I, Fatima T, Afzaal M, Ghuffar A. Synergistic GO/MgO nanocomposites with enhanced charge separation for photocatalytic dye degradation. *Explora Environ Resour*. 2026;3(1):025480080. doi: 10.36922/EER025480080

Received: November 24, 2025

Revised: December 11, 2025

Accepted: December 24, 2025

Published online: January 7, 2026

Metal oxide semiconductors, particularly TiO_2 and ZnO, have dominated photocatalysis research over the past decades. Recently, magnesium oxide (MgO) has garnered considerable attention due to its exceptional chemical stability, low toxicity, abundance on Earth, and unique surface basicity. The wide band gap of MgO (~5.0–5.5 eV) primarily limits its photocatalytic activity to the Ultraviolet (UV) region, while rapid electron–hole (e^-/h^+) recombination further diminishes the quantum efficiency. Therefore, strategic band gap engineering and improved charge-carrier utilization are imperative to unlock the full potential of MgO-based photocatalysts.[4,5]

Graphene oxide (GO), a two-dimensional carbon nanomaterial decorated with oxygen-containing functional groups (hydroxyl, epoxy, carbonyl, and carboxyl), has emerged as an efficient interfacial modifier for semiconductor photocatalysts due to its conjugated π-electron system and electron-acceptor characteristics.[6] The integration of GO with metal oxide semiconductors can enhance photocatalytic performance primarily by facilitating interfacial charge transfer and improving pollutant–catalyst contact, while also enabling modest tuning of optical absorption depending on the oxide system. Recent studies on GO-based binary composites with TiO_2, ZnO, and SnO_2 have reported substantial enhancements in photocatalytic activity. However, GO/MgO nanocomposites remain relatively underexplored despite their promising theoretical framework.[7-10] Ikram *et al*.[9] reported that GO-doped MgO nanostructures achieve rapid degradation of MB and ciprofloxacin under acidic conditions, demonstrating the potential of this system. Similarly, composite systems incorporating reduced GO with MgO have shown improved photocatalytic activity. Nevertheless, systematic investigations correlating GO content with structural, optical, and photocatalytic properties, coupled with mechanistic insights into interfacial charge-transfer behavior and optimization of operational parameters, remain limited.[11,12]

In this work, we present a comprehensive study on the synthesis, characterization, and photocatalytic evaluation of GO/MgO nanocomposites with systematically varied GO content (0, 0.01, 0.03, and 0.05 wt.%). We employed a facile co-precipitation method followed by thermal treatment to promote GO–MgO interfacial coupling. The structural, optical, and chemical properties were investigated using X-ray diffraction (XRD), UV–visible diffuse reflectance spectra (UV–vis DRS), Fourier transform infrared (FTIR), and Raman spectroscopy. The photocatalytic performance was evaluated through MB degradation under UV irradiation, with detailed kinetic analysis and parametric optimization (pH and catalyst dosage). Furthermore, post-reaction characterization was conducted to assess catalyst stability and reusability potential. Our results demonstrate that ultralow GO loading induces bandgap tuning and improved photocatalytic kinetics, suggesting improved charge-carrier utilization through interfacial electron transfer in the GO/MgO system.

2. Materials and methods

2.1. Materials

Magnesium nitrate hexahydrate ($Mg(NO_3)_2{\cdot}6H_2O$, ≥99%), sodium hydroxide (NaOH, ≥98%), and MB ($C_{16}H_{18}ClN_3S$, ≥95%) were procured from Sigma-Aldrich (United States [US]). GO aqueous dispersion (4 mg/mL, single-layer content >95%) was purchased from Graphenea (Spain). All chemicals were used as received without further purification. Deionized water (resistivity 18.2 MΩ·cm) was used throughout all experiments.

2.2. Synthesis of GO/MgO nanocomposites

GO/MgO nanocomposites were synthesized through a co-precipitation method adapted from the literature with modifications.[11] Briefly, appropriate volumes of GO dispersion were diluted in 50 mL of deionized water under vigorous stirring to achieve final GO concentrations of 0, 0.01, 0.03, and 0.05 wt.% relative to MgO. Subsequently, 0.1 M $Mg(NO_3)_2{\cdot}6H_2O$ solution (100 mL) was added dropwise to the GO suspension under continuous stirring at 60°C. The pH was maintained at 11–12 by dropwise addition of 2 M NaOH solution to ensure complete precipitation of $Mg(OH)_2$. The resulting suspension was aged for 2 h at 60°C with constant stirring, then cooled to room temperature and aged overnight. The precipitate was collected by centrifugation (8,000 rpm, 10 min; [Hettich EBA 20 centrifuge, Andreas Hettich GmbH, Germany]), washed thoroughly with deionized water and ethanol to remove residual ions, and dried at 80°C for 12 h. Finally, the dried powder was calcined at 550°C for 3 h in an air atmosphere (heating rate: 5°C/min) to obtain GO/MgO nanocomposites. The samples were designated as pure MgO, 0.01-GO/MgO, 0.03-GO/MgO, and 0.05-GO/MgO based on their GO content.

2.3. Characterization techniques

XRD patterns were recorded using a Bruker D8 Advance diffractometer (Germany) with Cu Kα radiation (λ = 1.54056 Å) operating at 40 kV and 40 mA. Diffraction data were collected over the range of 10–90° with a step size of 0.02° and a scan rate of 2°/min. The crystallite size

(D) was calculated from the most intense (200) reflection using the Scherrer equation:

$$D = \frac{K\lambda}{\beta\cos\theta} \quad (1)$$

where K is the shape factor (0.9), λ is the X-ray wavelength, β is the full width at half maximum (FWHM) in radians, and θ is the Bragg diffraction angle. The interplanar spacing (d) was obtained using Bragg's law:

$$d = \frac{\lambda}{2\sin\theta} \quad (2)$$

The lattice parameter (a) of cubic MgO was then determined using:

$$a = d\sqrt{h^2 + k^2 + l^2} \quad (3)$$

Microstrain (ε) was estimated using:

$$\varepsilon = \frac{\beta}{4\tan\theta} \quad (4)$$

and dislocation density (δ) was calculated as:

$$\delta = \frac{1}{D^2} \quad (5)$$

UV–visible diffuse reflectance spectra were obtained using a Shimadzu UV-2600 spectrophotometer (Japan) over the wavelength range of 200–800 nm with $BaSO_4$ as a reference standard. The optical band gap (E_g) was determined using Tauc plots for direct transitions according to:

$$(\alpha h\nu)^2 = A(h\nu - E_g) \quad (6)$$

where α is the absorption coefficient, $h\nu$ is the photon energy, and A is a constant. The band gap was estimated by extrapolating the linear region of $(\alpha h\nu)^2$ versus plots to the energy axis.

FTIR spectra were recorded on a PerkinElmer Spectrum Two spectrometer (US) in the range of 400–4,000 cm^{-1} using the KBr pellet method (sample: KBr = 1:100). Each spectrum was acquired with 32 scans at 4 cm^{-1} resolution. Raman spectroscopy was performed using a LabRAM HR Evolution spectrometer (Japan) with 532 nm laser excitation (power: 5 mW) to minimize sample heating. Spectra were recorded in the range of 100–3,200 cm^{-1} with an acquisition time of 30 s and three accumulations.

2.4. Photocatalytic activity evaluation

Photocatalytic degradation experiments were conducted using MB as a model pollutant under UV irradiation. In a typical experiment, 50 mg of photocatalyst was dispersed in 100 mL of MB aqueous solution (15 mg/L) in a cylindrical quartz reactor. Before irradiation, the suspension was magnetically stirred in the dark for 30 min to establish adsorption–desorption equilibrium. The reactor was then exposed to UV light (λ = 365 nm, 36 W mercury lamp positioned 10 cm above the solution surface) under continuous stirring. At predetermined time intervals (0, 15, 30, 45, 60, 90, 120, 150, and 180 min), 3 mL aliquots were withdrawn, centrifuged (10,000 rpm, 5 min) to remove catalyst particles, and analyzed using UV–Vis spectroscopy (Shimadzu UV-1800) at λ_{max} = 664 nm. The degradation efficiency was calculated using the following equation:

$$\text{Degradation (\%)} = \frac{C_0 - C_t}{C_0} \times 100 \quad (7)$$

Where C_0 is the initial concentration and C_t is the concentration at time t after adsorption equilibrium. All experiments were performed in triplicate, and average values with standard deviations are reported. For kinetic analysis, the pseudo-first-order model was applied using:

$$\ln\left(\frac{C_0}{C_t}\right) = kt \quad (8)$$

where k is the apparent rate constant (min^{-1}) and t is the irradiation time (min).

2.5. Effect of operational parameters

The influence of solution pH (3, 5, 7, 9, and 11) and catalyst dosage (0.2, 0.3, 0.5, 0.75, and 1.0 g/L) on photocatalytic performance was systematically investigated using the optimal 0.05-GO/MgO catalyst. pH adjustments were made using 0.1 M HCl or NaOH solutions before catalyst addition. All other experimental conditions remained constant as described above.

2.6. Catalyst stability assessment

To evaluate the structural and chemical stability, the 0.05-GO/MgO catalyst was recovered after the photocatalytic reaction (180 min), thoroughly washed with deionized water and ethanol, dried at 80°C overnight, and then subjected to XRD and FTIR analysis. The pre- and post-reaction characterization data were compared to assess any structural or compositional changes that may have occurred during the reaction.

3. Results and discussion

3.1. Structural analysis

3.1.1. XRD

Figure 1 presents the XRD patterns of pure MgO and GO/MgO nanocomposites. All samples exhibited

characteristic diffraction peaks at 2θ ≈ 37.0°, 43.0°, 62.5°, 74.7°, and 78.8°, corresponding to the (111), (200), (220), (311), and (222) crystallographic planes of cubic MgO (space group: $Fm\bar{3}m$, JCPDS card no. 45-0946). The absence of secondary phases confirms successful incorporation of GO into the MgO matrix without compromising phase purity. Notably, the characteristic GO (001) peak expected at 2θ ≈ 10–11° appeared as a weak, broad feature in GO-containing samples, becoming more pronounced with increasing GO content, consistent with literature reports.[13-15]

A slight shift of the (200) peak to lower 2θ values was observed with increasing GO content (43.30° for pure MgO–42.94° for 0.05-GO/MgO). However, this shift was modest and did not provide conclusive evidence for carbon entering the MgO lattice. Considering the small magnitude of this change and the lack of a clearly systematic shift of comparable scale across other major MgO reflections, the observed variation is more reasonably attributed to interfacial strain and microstructural effects associated with GO–MgO coupling, along with crystallite-size-related broadening. Concurrently, progressive peak broadening was evident, suggesting crystallite size reduction.

Quantitative structural parameters extracted from XRD data are summarized in Table 1. The crystallite size, calculated using the Scherrer equation (Equation [1]) from the (200) reflection, decreased systematically from 20.26 nm for pure MgO to 13.26 nm for 0.05-GO/MgO. This reduction is attributed to GO sheets acting as nucleation sites and physical barriers that restrict the growth of MgO crystals during the synthesis process. The lattice parameter increased marginally from 4.204 Å (pure MgO) to 4.209 Å (0.05-GO/MgO), corroborating the peak shift observations. Microstrain values increased from 1.711 × 10^{-3} (pure MgO) to 2.613 × 10^{-3} (0.05-GO/MgO), while dislocation

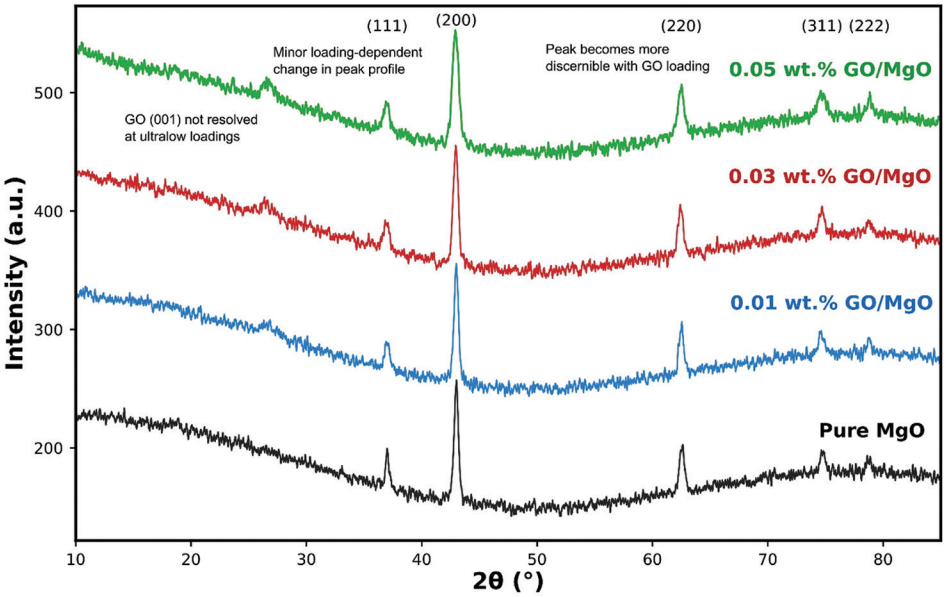

Figure 1. X-ray diffraction patterns of pure magnesium oxide (MgO) and graphene oxide (GO)/MgO nanocomposites with ultralow GO loadings (0.01, 0.03, and 0.05 wt.%). All samples exhibit the characteristic reflections of cubic MgO, confirming phase retention across the series. The respective patterns are labeled according to GO loading to highlight the loading-dependent evolution of diffraction profiles. Any GO-related reflection is weak or not clearly resolved at these ultralow contents, consistent with composite formation dominated by interfacial coupling rather than the emergence of additional crystalline phases.

Table 1. Structural parameters of GO/MgO nanocomposites derived from X-ray diffraction analysis

Sample	2θ (200) (°)	FWHM (°)	d-spacing (Å)	Crystallite size (nm)	Lattice parameter (Å)	Microstrain (× 10^{-3})	Dislocation density (× 10^{15} m^{-2})
Pure MgO	43.30	0.421	2.102	20.26	4.204	1.711	2.437
0.01-GO/MgO	43.30	0.480	2.102	17.79	4.204	1.948	3.159
0.03-GO/MgO	43.25	0.501	2.104	17.03	4.208	2.036	3.450
0.05-GO/MgO	42.94	0.644	2.105	13.26	4.209	2.613	5.684

Abbreviation: FWHM: Full width at half maximum; GO/MgO: Graphene oxide–magnesium oxide.

density rose from 2.437 × 10^{15} m^{-2} to 5.684 × 10^{15} m^{-2}, indicating enhanced lattice distortions and defect density with GO incorporation. These structural defects can potentially serve as charge-trapping sites, influencing the photocatalytic performance.

3.1.2. UV–visible diffuse reflectance spectroscopy

Figure 2A displays the UV–vis DRS absorption spectra of all samples. Pure MgO exhibited a sharp absorption edge at ~243 nm, characteristic of its wide band gap. GO incorporation induced a systematic red shift of the absorption edge and enhanced visible light absorption, particularly evident in the 0.05-GO/MgO sample. This extended absorption can be attributed to: (i) charge transfer transitions between MgO and GO, (ii) introduction of defect states within the band gap, and (iii) light scattering effects from the GO–MgO heterojunction.[16]

Band gap energies determined from Tauc plots (Figure 2B) are presented in Table 2. Pure MgO exhibited a band gap of 5.11 eV, consistent with literature values. Progressive GO loading resulted in substantial band gap narrowing: 5.01 eV (0.01-GO/MgO), 4.76 eV (0.03-GO/MgO), and 4.71 eV (0.05-GO/MgO)—a total reduction of 0.40 eV (7.8%). This narrowing is attributed to the formation of intermediate energy states arising from GO's oxygen-containing functional groups and the π-conjugated carbon network, both of which create electronic coupling with MgO. The red shift of 20.46 nm for 0.05-GO/MgO corresponds to improved visible light harvesting capacity, potentially enhancing photocatalytic activity under solar irradiation.[17]

3.2. Chemical bonding and surface analysis

3.2.1. FTIR spectroscopy

The FTIR spectra (Figure 3) provided crucial insights into the chemical structure and bonding environment of GO/MgO nanocomposites. All samples displayed characteristic Mg–O stretching vibrations at 443 cm^{-1} and 594 cm^{-1}, confirming the formation of MgO. Surface hydroxyl groups were evident from the sharp peak at 3,699 cm^{-1} and the broad band centered at 3,340 cm^{-1}, attributed to Mg–OH stretching and adsorbed water molecules, respectively. The intensity of these peaks decreased with increasing GO content, suggesting that GO sheets wrap around MgO nanoparticles, thereby reducing the exposed MgO surface area, which is consistent with XRD crystallite size observations.[18,19]

GO-specific functional groups emerged progressively with increasing GO content. The peaks at 1,727 cm^{-1} (C=O stretching of carbonyl/carboxyl groups), 1,623 cm^{-1} (C=C stretching of aromatic sp^2 carbon), 1,398 cm^{-1} (C–OH deformation), 1,132 cm^{-1} (C–O stretching of epoxy groups), and the band near 964 cm^{-1} (C–O–C-related vibrations) indicate the retention of oxygen-rich functionalities associated with GO after thermal treatment at 550°C. The appearance and gradual intensification of the ~964 cm^{-1} feature with increasing GO loading is consistent with strengthened interfacial interactions between GO functional groups and MgO surface sites. However, in the absence of the FTIR spectrum of pristine GO and without XPS analysis, this assignment should be regarded as suggestive rather than definitive evidence of a specific covalent bonding motif. Such interfacial contact is expected to promote more efficient electron transfer across the heterojunction interface, contributing to the enhanced photocatalytic performance.[20] Carbonate-related peaks at 1,450 cm^{-1} (C–O asymmetric stretching) and 865 cm^{-1} (O–C–O bending) were observed in all samples, arising from atmospheric CO_2 adsorption on the basic MgO surface. Interestingly, these peaks diminished with the increase in GO loading, indicating that GO sheets may partially shield the MgO surface and reduce carbonate formation.

3.2.2. Raman spectroscopy

Raman spectroscopy was employed to probe the carbon structure and graphitic quality of GO in the nanocomposites (Figure 4A). Pure MgO exhibited weak features at ~275 cm^{-1} and ~447 cm^{-1}, corresponding to MgO transverse optical and longitudinal optical phonon modes, respectively. These peaks were largely obscured in GO-containing samples due to the strong Raman scattering from GO.[21]

GO-doped samples displayed two prominent bands: The D band at ~1,338 cm^{-1} (A_1g breathing mode of sp^3 carbon atoms and structural defects) and the G band at ~1,598 cm^{-1} (E_2g phonon of sp_2 carbon networks). The D-band intensity increased with the GO content, confirming GO incorporation. The I_D/I_G ratio is a critical parameter for assessing graphitic disorder and crystalline quality. As shown in Figure 4B, our results (Table 3) revealed a decreasing trend: 0.886 (0.01-GO/MgO) → 0.866 (0.03-GO/MgO) → 0.830 (0.05-GO/MgO). This 6.3% reduction indicates improved ordering of sp^2 carbon domains at higher GO concentrations, suggesting that GO sheets self-organize more effectively when present at sufficient loading, facilitating better π-electron delocalization. This enhanced electronic structure is favorable for electron transport and charge separation in photocatalysis.[22-24]

The slight upshift of the G band position (1606.5 → 1611.5 cm^{-1}) with increasing GO content suggests compressive strain arising from GO–MgO interfacial

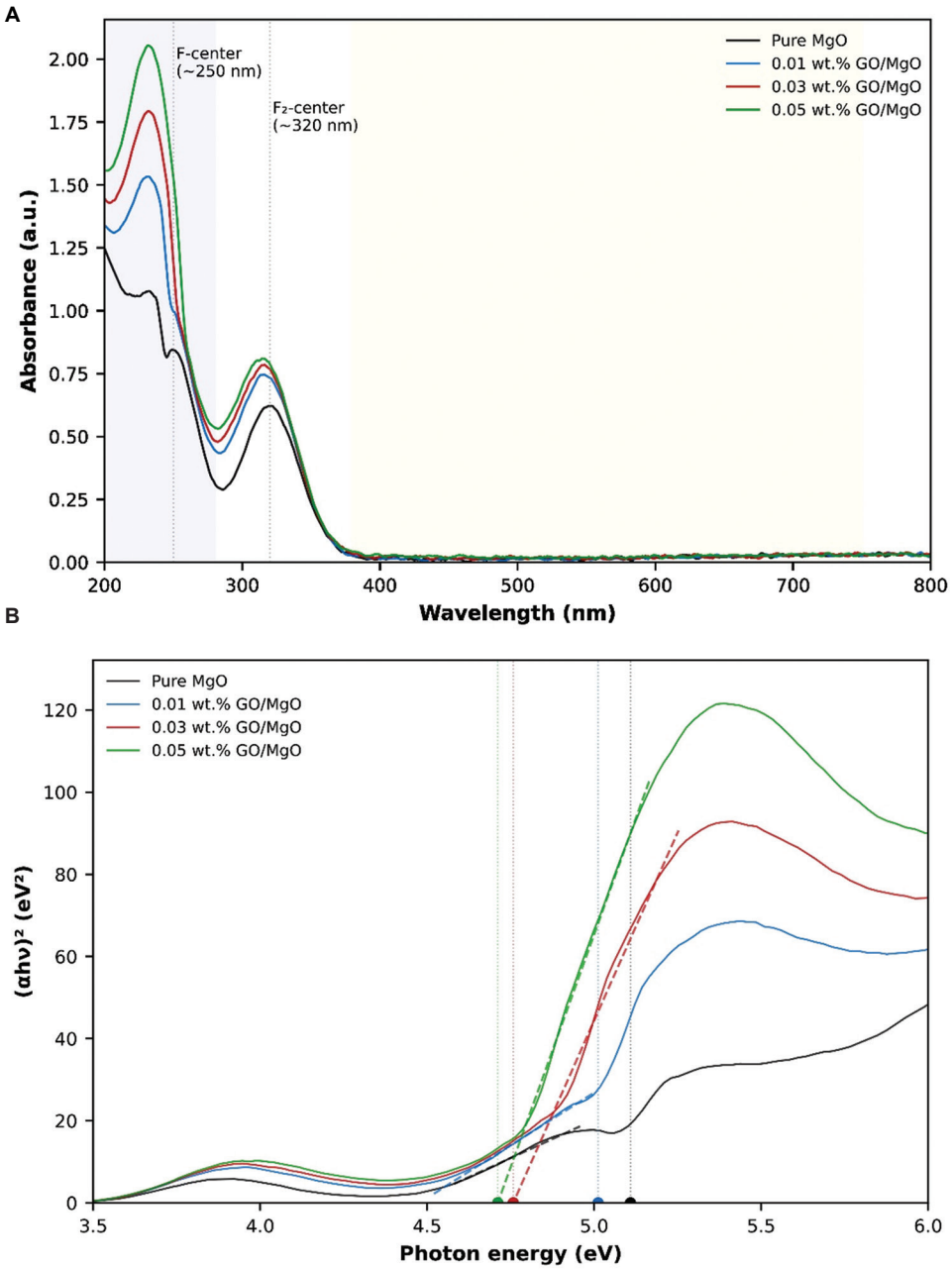

Figure 2. Optical properties of graphene oxide (GO)–magnesium oxide nanocomposites. (A) Ultraviolet–visible diffuse reflectance spectra showing a red shift with GO loading. (B) Tauc plots for band gap determination using the direct transition model.

Table 2. Optical properties correlated with X-ray diffraction-derived structural parameters of GO/MgO nanocomposites

Sample	GO loading (wt.%)	Absorption edge (nm)	Red shift (nm)	Band gap (eV)	Band gap reduction (eV)	Crystallite size (nm)	Lattice parameter (Å)	Microstrain ($\times 10^{-3}$)	Dislocation density ($\times 10^{15}$ m^{-2})
Pure MgO	0	243	0.00	5.109	0.000	20.26	4.204	1.711	2.437
0.01-GO/MgO	0.01	247	4.69	5.012	0.097	17.79	4.204	1.948	3.159
0.03-GO/MgO	0.03	261	17.90	4.758	0.351	17.03	4.208	2.036	3.450
0.05-GO/MgO	0.05	263	20.46	4.711	0.397	13.26	4.209	2.613	5.684

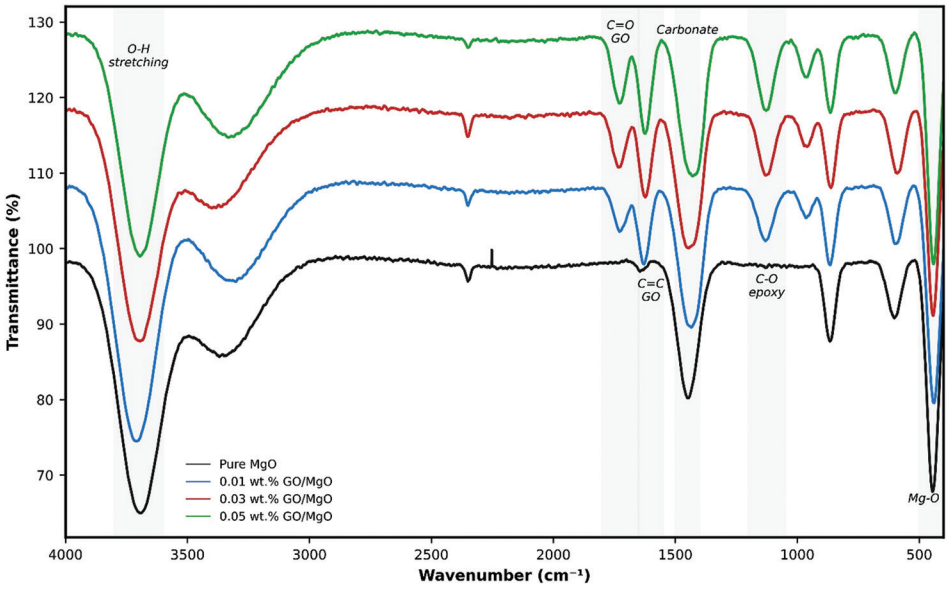

Figure 3. Fourier-transform infrared spectra of graphene oxide–magnesium oxide nanocomposites highlighting key functional groups

Table 3. Raman spectroscopy analysis of GO/MgO nanocomposites

Sample	D-band position (cm^{-1})	G-band position (cm^{-1})	I_D/I_G ratio	$FWHM_D$ (cm^{-1})	$FWHM_G$ (cm^{-1})
0.01-GO/MgO	1,330.4	1,606.5	0.886	77.8	71.2
0.03-GO/MgO	1,343.4	1,608.5	0.866	83.3	71.4
0.05-GO/MgO	1,345.4	1,611.5	0.830	84.1	69.5

Abbreviations: GO/MgO: Graphene oxide–magnesium oxide; FWHM: Full width at half maximum.

interactions, corroborating XRD findings of lattice expansion and increased microstrain.

The formation of GO/MgO nanocomposites in this study is inferred from the designed co-precipitation route and the consistent, loading-dependent convergence of structural, optical, and vibrational signatures. XRD confirms retention of the cubic MgO phase with systematic microstructural evolution on GO loading, while FTIR and Raman spectra reveal GO-related functional and graphitic features that evolve progressively with composition. The accompanying red shift and bandgap reduction, together with the monotonic enhancement in the apparent rate constant across the GO series, further support the presence of an interfacially coupled GO–MgO system rather than a simple physical mixture. In the absence of direct morphological imaging, these multi-technique correlations provide coherent evidence for composite formation dominated by interfacial coupling.

3.3. Photocatalytic performance

3.3.1. MB degradation kinetics

The photocatalytic activity of GO/MgO nanocomposites was evaluated through MB degradation under UV irradiation. Figure 5A presents the temporal evolution of relative MB concentration (C/C_0) for all samples. Pure MgO achieved only 44.3% degradation after 180 min, reflecting its wide band gap and high charge recombination rate. GO incorporation dramatically enhanced photocatalytic performance: 61.8% (0.01-GO/MgO), 82.5% (0.03-GO/MgO), and 91.6% (0.05-GO/MgO). The 0.05-GO/MgO catalyst demonstrated a 2.07-fold improvement in degradation efficiency compared to pure MgO.

Kinetic analysis (Figure 5B) revealed excellent adherence to pseudo-first-order kinetics ($R^2 > 0.98$), as evidenced by the linear relationship between $\ln(C_0/C_t)$ and irradiation time. The apparent rate constants (k) increased systematically with GO content (Table 4): 0.00290 min^{-1} (pure MgO), 0.00527 min^{-1} (0.01-GO/MgO), 0.00910 min^{-1} (0.03-GO/MgO), and 0.01518 min^{-1} (0.05-GO/MgO). The 0.05-GO/MgO catalyst exhibited a remarkable 5.24-fold enhancement in rate constant relative to pure MgO, corresponding to a half-life reduction from 239.1 min to 45.7 min.

These results surpass several recent reports on metal oxide-graphene composites. For example, GO/ZnO

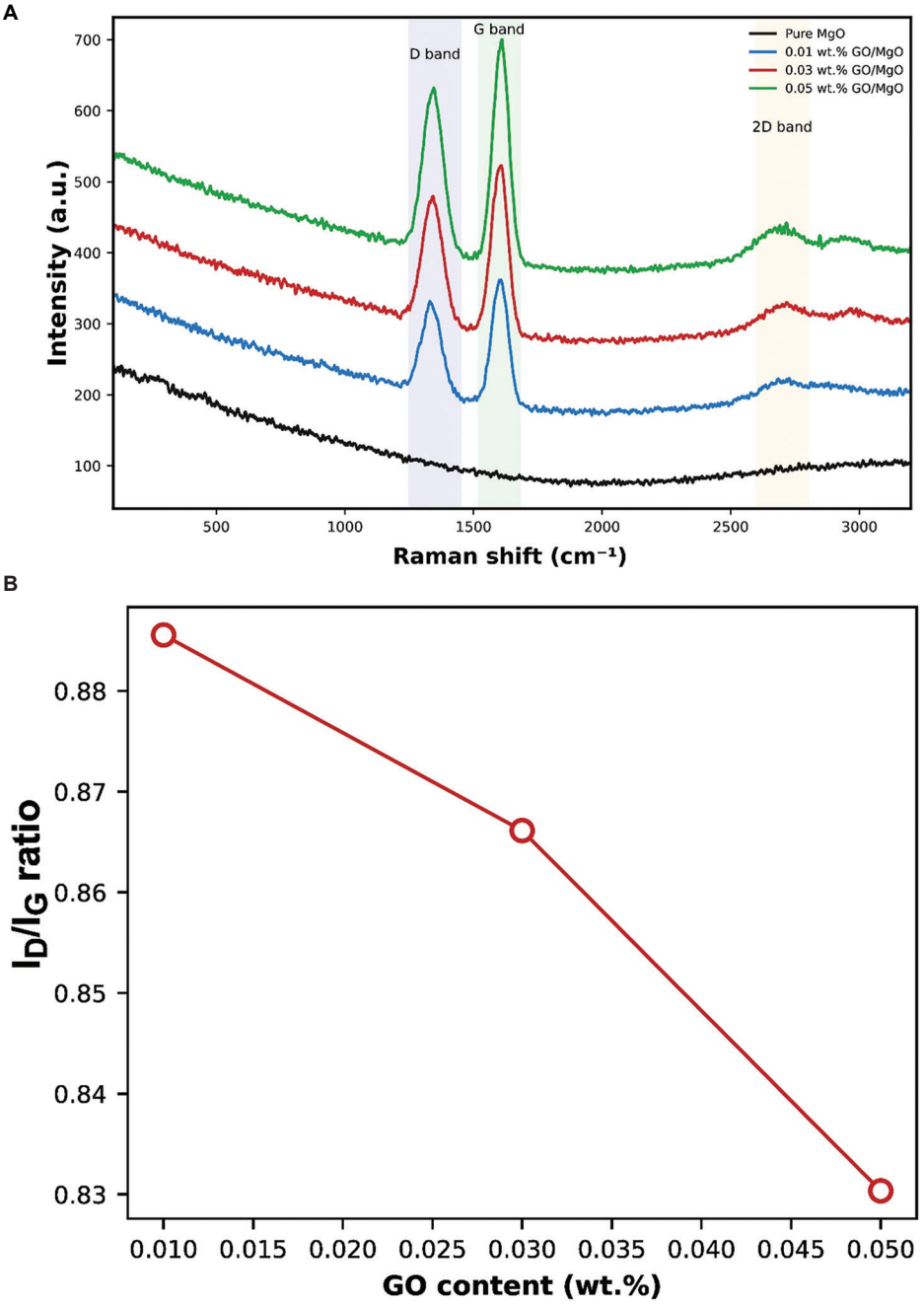

Figure 4. Raman spectroscopic analysis of graphene oxide (GO)/magnesium oxide nanocomposites. (A) Raman spectra showing D and G bands for GO-containing samples. (B) Variation of the I_D/I_G ratio as a function of GO content, demonstrating improved sp^2 ordering.

Table 4. Kinetic parameters for methylene blue photodegradation

Sample	Rate constant k (min^{-1})	Half-life $t_{1/2}$ (min)	Degradation at 180 min (%)	R^2	Enhancement factor
Pure MgO	0.00290	239.1	44.3	0.9909	1.00
0.01-GO/MgO	0.00527	131.6	61.8	0.9951	1.82
0.03-GO/MgO	0.00910	76.2	82.5	0.9874	3.14
0.05-GO/MgO	0.01518	45.7	91.6	0.9845	5.24

Abbreviation: GO/MgO: Graphene oxide–magnesium oxide.

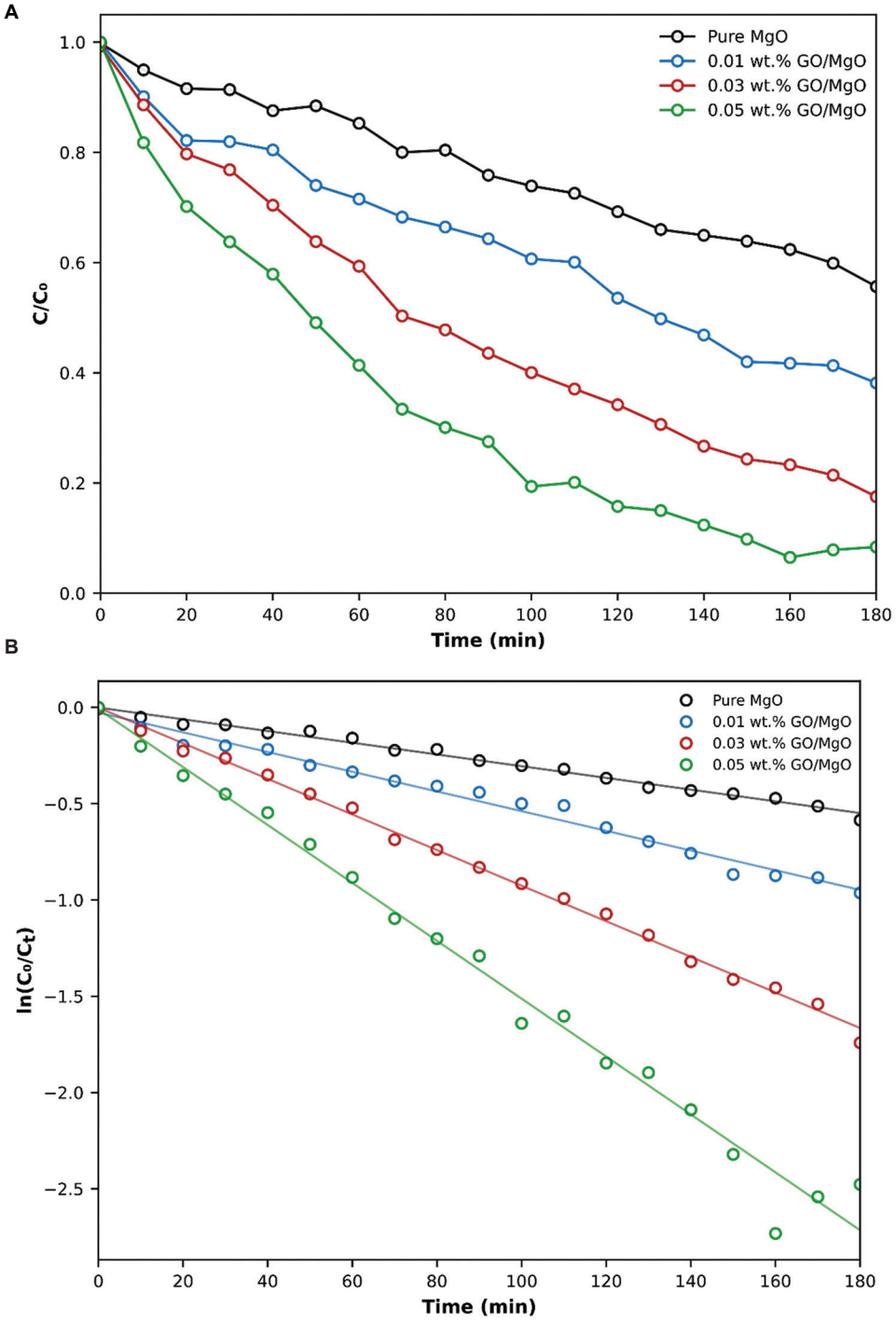

Figure 5. Photocatalytic degradation kinetics of methylene blue over graphene oxide–magnesium oxide nanocomposites. (A) Degradation curves (C/C_0 vs. time) for methylene blue photocatalysis. (B) Pseudo-first-order kinetic plots, $\ln(C_0/C_t)$ versus irradiation time, with linear fits and corresponding rate constants.

nanocomposites achieved 3.2-fold enhancement in rhodamine B degradation, while GO/TiO_2 showed 4.1-fold improvement in methyl orange removal.[9,25] Our 5.24-fold enhancement in the apparent rate constant positions GO/MgO among the most effective graphene-metal oxide photocatalysts reported to date. The superior performance can be attributed to the synergistic combination of: (i) narrowed band gap enabling enhanced

photon absorption (Figure 2), (ii) reduced crystallite size potentially increasing the density of accessible reactive sites (Table 1), (iii) efficient electron scavenging by GO sheets minimizing recombination, and (iv) intimate interfacial contact/interactions facilitating rapid charge transfer (suggested by FTIR features including the band near 964 cm^{-1}).

3.3.2. Effect of solution pH

Solution pH has a critical influence on photocatalytic processes through multiple mechanisms: catalyst surface charge, pollutant speciation, and reactive species generation. Figure 6 illustrates the pH dependence of MB degradation over 0.05-GO/MgO. Optimal performance was observed in the pH range of 7–9, achieving 94.9–95.8% degradation with rate constants of 0.01669–0.01965 min^{-1}. Degradation efficiency decreased at both acidic (pH 3: 83.4%) and strongly alkaline (pH 11: 91.2%) conditions.

The pH-dependent behavior can be rationalized as follows. At acidic pH, the MgO surface becomes protonated ($Mg–OH_2^+$), generating electrostatic repulsion with cationic MB molecules ($pK_a \approx 3.8$), hindering adsorption. In addition, reduced hydroxyl radical (–OH) generation occurs due to lower OH^- availability. At neutral-to-slightly alkaline pH (7–9), the surface carries a moderate negative charge ($Mg–O^-$), facilitating MB adsorption while maintaining efficient –OH production. At a strongly alkaline pH (≥11), excessive OH^- ions compete for active sites and may deactivate photogenerated holes through direct reaction, diminishing oxidative potential. Our results align with reports on MgO-based photocatalysts, where near-neutral pH typically yields optimal performance.[26,27]

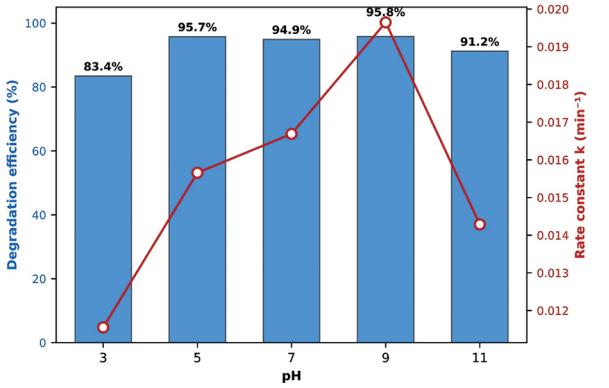

Figure 6. Effect of solution pH on photocatalytic degradation efficiency and rate constant for 0.05-graphene oxide–magnesium oxide catalyst

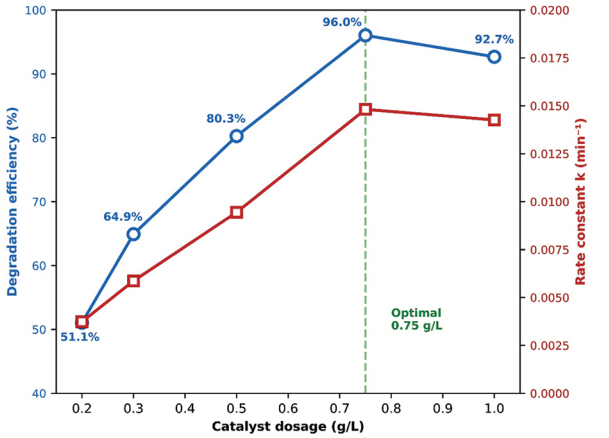

Figure 7. Effects of catalyst dosage on methylene blue photodegradation efficiency and rate constant. Dual-axis plot showing optimization at 0.75 g/L.

3.3.3. Effect of catalyst dosage

Catalyst dosage optimization balances active site availability with light penetration (Figure 7). Degradation efficiency increased progressively with catalyst dosage: 47.1% (0.2 g/L), 61.9% (0.3 g/L), 79.4% (0.5 g/L), reaching a maximum at 0.75 g/L (94.4%). Further increase to 1.0 g/L caused a slight decline to 92.9%.

The initial enhancement stems from increased availability of active sites and photon absorption. However, excessive catalyst loading (>0.75 g/L) increases solution turbidity, reducing photon penetration depth and creating light-screening effects that limit photocatalytic efficiency—a well-documented phenomenon. The optimal dosage of 0.75 g/L represents a practical compromise between catalytic activity and economic considerations.[28,29]

3.4. Photocatalytic mechanism

Figure 8 schematically illustrates the proposed charge transfer mechanism in GO/MgO nanocomposites. Under UV irradiation ($h\nu \geq E_g$), photons are absorbed by MgO, promoting electrons from the valence band (VB) to the conduction band (CB), leaving behind holes:

$$MgO + h\nu \rightarrow e^-_{CB} + h^+_{VB}$$

In pure MgO, rapid e^-/h^+ recombination limits photocatalytic efficiency. GO introduction provides an efficient electron sink due to its work function (~4.9 eV) being lower than MgO's CB position (~−2.3 eV vs. normal hydrogen electrode). Photogenerated electrons spontaneously transfer from MgO CB to GO sheets, driven by this energetic gradient:[30]

$$e^-_{CB(MgO)} \rightarrow GO$$

This charge separation is potentially facilitated by interfacial contact between MgO and GO. The FTIR evolution of the band near 964 cm^{-1} is consistent with such interactions, although direct identification of

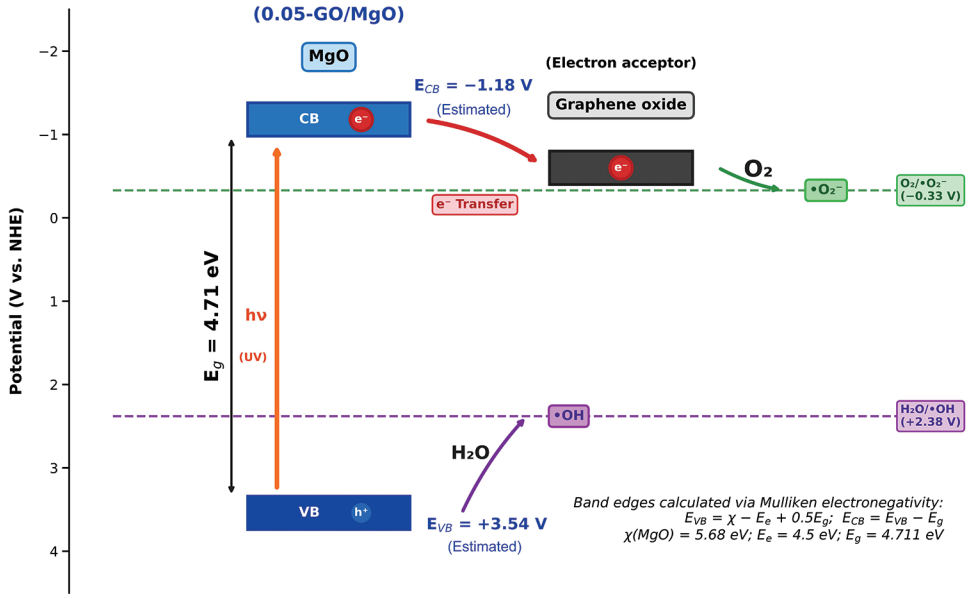

Figure 8. Proposed photocatalytic mechanism of the 0.05-GO/MgO nanocomposite for methylene blue (MB) degradation under ultraviolet (UV) irradiation. The MgO band-edge positions (estimated vs. NHE; E_{CB} = −1.18 V and E_{VB} = +3.54 V) are shown alongside key redox potentials ($O_2/\bullet O_2^-$ = −0.33 V and $H_2O/\bullet OH$ = +2.38 V) using the measured optical band gap (E_g = 4.71 eV). Upon UV excitation, electrons are promoted from the VB to the CB, generating e^-/h^+ pairs (MgO + hν → $e^-_{(CB)}$ + $h^+_{(VB)}$). GO is proposed to act as an electron acceptor, facilitating interfacial charge transfer ($e^-_{(MgO)} \rightarrow e^-_{(GO)}$) and suppressing charge recombination. The transferred electrons reduce dissolved oxygen to superoxide radicals ($O_2 + e^- \rightarrow \bullet O_2^-$), while VB holes oxidize surface H_2O/OH^- to hydroxyl radicals ($H_2O/OH^- + h^+ \rightarrow \bullet OH$). The resulting reactive oxygen species ($\bullet O_2^-/\bullet OH$) subsequently oxidize MB to degradation products.
Abbreviations: CB: Conduction band; NHE: Normal hydrogen electrode; VB: Valence band; GO: Graphene oxide; MgO: Magnesium oxide.

specific bonding motifs would require XPS or related surface-sensitive analysis. The trapped electrons on GO subsequently reduce molecular oxygen to form superoxide radicals:

$$GO(e^-) + O_2 \rightarrow GO + O_2^-$$

Simultaneously, photogenerated holes in MgO VB oxidize water or hydroxyl ions to generate hydroxyl radicals:

$$h^+_{VB} + H_2O \rightarrow H^+ + OH$$

$$h^+_{VB} + OH^- \rightarrow OH$$

These reactive oxygen species (–OH and $-O_2^-$) are powerful oxidants that react with MB molecules, cleaving chromophoric bonds and ultimately mineralizing the dye:

$$MB + (OH, O_2^-, h^+) \rightarrow Intermediates \rightarrow CO_2 + H_2O + \text{mineral acids}$$

The synergistic enhancements observed in our study, narrowed band gap (UV–vis DRS), reduced crystallite size (XRD), interfacial bonding (FTIR), and improved sp^2 ordering (Raman spectrometry), collectively contribute to the exceptional 5.24-fold rate enhancement by: (i) Increasing photon absorption efficiency, (ii) potentially increasing the density of accessible reactive sites, (iii) accelerating interfacial electron transfer, and (iv) likely suppressing charge recombination through interfacial electron transfer to GO. This mechanism is consistent with electron paramagnetic resonance studies on similar GO-metal oxide systems, which confirmed –OH and $-O_2^-$ as primary reactive species.[31] Although XRD indicates crystallite refinement with GO incorporation, direct visualization and quantitative surface area analysis (scanning electron microscopy [SEM]/transmission electron microscopy [TEM] and Brunauer–Emmett–Teller [BET] method) were not available in the present study; therefore, claims related to surface-area-driven active-site enhancement are stated as potential inferences based on crystallite-size trends. In addition, direct verification of charge-separation behavior through photoluminescence (PL), transient photocurrent, or electrochemical impedance spectroscopy (EIS) was not performed in the present study; therefore, the recombination–suppression mechanism is presented as a supported inference based on kinetic enhancement and interfacial/optical trends.

3.5. Catalyst stability and reusability

Long-term stability is paramount for practical photocatalytic applications. We assessed the structural

and chemical integrity of 0.05-GO/MgO after 180 min of photocatalytic reaction through comparative XRD and FTIR analysis (Figure 9).

The XRD patterns (Figure 9A) of the post-reaction catalyst exhibited no new crystalline phases, confirming the cubic MgO structure remained intact. Peak positions were unchanged, indicating no phase transformation or chemical degradation occurred. A marginal FWHM increase (~8%) was observed for the (200) reflection, suggesting minor surface amorphization attributable to prolonged UV exposure and interaction with the aqueous environment, a common phenomenon that is not detrimental to photocatalytic activity. The crystallite size decreased slightly to ~12.2 nm (from 13.26 nm), within the experimental variation. FTIR analysis (Figure 9B) revealed that characteristic Mg–O vibrations (443 and 594 cm^{-1}) and GO functional groups (1,727, 1,623, 1,132, and 964 cm^{-1}) were preserved at >96% intensity, confirming

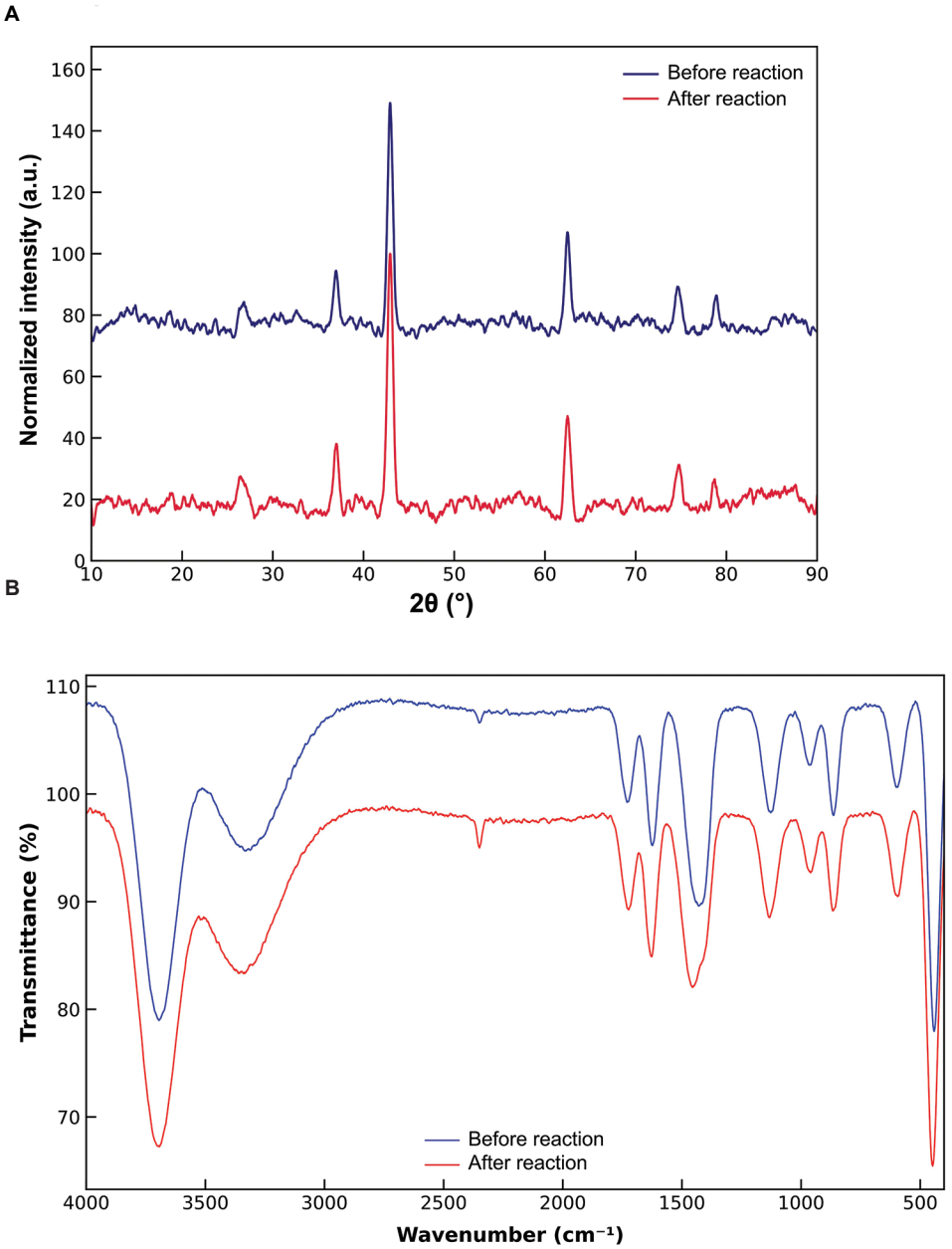

Figure 9. Comparative characterization of the optimized 0.05-GO/MgO catalyst before and after photocatalytic reaction. (A) X-ray diffraction patterns indicate the retention of the cubic MgO phase. (B) Fourier-transform infrared spectra show no significant loss of the main functional-group features. These results suggest excellent structural and chemical stability of the catalyst under the applied reaction conditions.

the GO–MgO heterojunction remained stable. A slight increase (12–15%) in hydroxyl peak intensity (3,699 and 3,340 cm^{-1}) was attributed to enhanced water adsorption during aqueous reaction. Carbonate peaks showed 8–10% reduction, potentially due to surface cleaning effects during photocatalytic processes. These results demonstrate excellent structural and chemical stability of GO/MgO nanocomposites under operational conditions, suggesting potential for multiple reuse cycles without significant performance degradation. While comprehensive recyclability studies involving multiple degradation cycles are beyond the current scope, our stability assessment indicates promising reusability characteristics—a critical advantage for sustainable wastewater treatment applications.

4. Conclusion

GO–MgO nanocomposites with ultralow GO loadings (0–0.05 wt.%) were successfully synthesized through a co-precipitation route and evaluated for UV-driven MB degradation. XRD confirmed the retention of the cubic MgO phase across the series, while crystallite size decreased progressively from 20.26 nm for pristine MgO to 13.26 nm for 0.05-GO/MgO, indicating GO-assisted microstructural refinement. UV–vis DRS revealed a clear red shift and bandgap reduction from 5.109 eV to 4.711 eV with increasing GO content, suggesting an improved light-harvesting capability. FTIR and Raman spectra showed GO-related functional and graphitic signatures, indicating interfacial interactions that evolve systematically with GO loading. Photocatalytic experiments demonstrated a substantial loading-dependent enhancement in activity, with the optimized 0.05-GO/MgO sample achieving 91.6% MB degradation within 180 min. Kinetic analysis confirmed pseudo-first-order behavior, and the apparent rate constant increased from 0.00290 min^{-1} (pure MgO) to 0.01518 min^{-1} (0.05-GO/MgO), corresponding to a 5.24-fold enhancement. Performance was maximized at pH 7–9 with a catalyst dosage of 0.75 g/L, and post-reaction XRD/FTIR analysis indicated excellent structural stability of the optimized catalyst. Overall, the enhancement is attributed to the combined effects of crystallite refinement, bandgap tuning, and GO–MgO interfacial charge-transfer pathways, as inferred from consistent structural/optical–kinetic correlations. Direct morphological visualization and advanced charge-transport measurements (e.g., SEM/TEM, BET, and PL/EIS) will be pursued in future work to further refine the mechanistic understanding.

Acknowledgments

None.

Funding

None.

Conflict of interest

The authors declare that they have no competing interests.

Author contributions

Conceptualization: Irfan Toqeer
Formal analysis: Muhammad Afzaal
Investigation: Abdul Ghuffar
Methodology: Irfan Toqeer, Tahreem Fatima
Writing–original draft: Irfan Toqeer
Writing–review & editing: All authors

Ethics approval and consent to participate

Not applicable.

Consent for publication

Not applicable.

Availability of data

The data that support the findings of this study are available from the corresponding author on reasonable request.

References

1. Kuruthukulangara N, Thirumalai D, Asharani I. Eco-friendly synthesis and photocatalytic application of rGO-MgO nanocomposites for eosin Y dye degradation. *Chem Phys Impact*. 2025;11:100939.

   doi: 10.1016/j.chphi.2025.100939

2. Khurshid F, Jeyavelan M, Nagarajan S. Photocatalytic dye degradation by graphene oxide doped transition metal catalysts. *Synth Met*. 2021;278:116832.

   doi: 10.1016/j.synthmet.2021.116832

3. Pasindu V, Yapa P, Dabare S, Munaweera I. Multifunctional transition metal oxide/graphene oxide nanocomposites for catalytic dye degradation, renewable energy, and energy storage applications. *RSC Adv*. 2025;15(40):33162-33186.

   doi: 10.1039/D5RA04806K

4. Jaramillo-Fierro X, Cuenca G. Enhancing methylene blue removal through adsorption and photocatalysis-a study on the GO/$ZnTiO_3$/TiO_2 composite. *Int J Mol Sci*. 2024;25(8):4367.

   doi: 10.3390/ijms25084367

5. Ahmed MA, Mahmoud SA, Mohamed AA. Interfacially engineered metal oxide nanocomposites for enhanced photocatalytic degradation of pollutants and energy applications. *RSC Adv*. 2025;15(20):15561-15603.

   doi: 10.1039/D4RA08780A

6. Gatou MA, Bovali N, Lagopati N, *et al*. MgO nanoparticles as a promising photocatalyst towards rhodamine B and rhodamine 6G degradation. *Molecules*. 2024;29(18):4299.

doi: 10.3390/molecules29184299

7. Al-Rawashdeh NA, Allabadi O, Aljarrah MT. Photocatalytic activity of graphene oxide/zinc oxide nanocomposites with embedded metal nanoparticles for the degradation of organic dyes. *ACS Omega*. 2020;5(43):28046-28055.

doi: 10.1021/acsomega.0c03652

8. Sahoo S, Bhuyan M, Sahu AK, Alagarsamy P, Sahoo D. Photodegradation of methylene blue by metal-nanoparticles-modulated graphene-based composites. *Solid State Sci*. 2023;142:107255.

doi: 10.1016/j.solidstatesciences.2023.107255

9. Ikram M, Inayat T, Haider A, *et al*. Graphene oxide-doped MgO nanostructures for highly efficient dye degradation and bactericidal action. *Nanoscale Res Lett*. 2021;16(1):56.

doi: 10.1186/s11671-021-03510-3

10. Sarojini P, Leeladevi K, Kavitha T, *et al*. Design of V_2O_5 blocks decorated with garlic peel biochar nanoparticles: A sustainable catalyst for the degradation of methyl orange and its antioxidant activity. *Materials (Basel)*. 2023;16(17):5800.

doi: 10.3390/ma16175800

11. Mosleh AT, Hassan AE, Sabry N, *et al*. Design of MgO/graphene nanocomposites for photocatalytic reduction of 4-nitrophenol. *Phys Scr*. 2024;99(12):125914.

doi: 10.1088/1402-4896/ad8381

12. Tung CH, Chang JH, Hsieh YH, *et al*. Comparison of hydroxyl radical yields between photo- and electro-catalyzed water treatments. *J Taiwan Inst Chem Eng*. 2014;45(4):1649-1654.

doi: 10.1016/j.jtice.2013.11.011

13. Liyanaarachchi H, Thambiliyagodage C, Jayanetti M, Ekanayake G, Wijayawardana S, Samarakoon U. The photocatalytic and antibacterial activity of graphene oxide coupled CoOx/MnOx nanocomposites. Environ Technol Innov. 2025;37:103984.

doi: 10.1016/j.eti.2024.103984

14. Jamjoum HAA, Umar K, Adnan R, Razali MR, Mohamad Ibrahim MN. Synthesis, characterization, and photocatalytic activities of graphene oxide/metal oxides nanocomposites: A review. *Front Chem*. 2021;9:752276.

doi: 10.3389/fchem.2021.752276

15. Heidarizad M, Şengör SS. Synthesis of graphene oxide/magnesium oxide nanocomposites for adsorption of methylene blue. *J Mol Liq*. 2016;224:607-617.

doi: 10.1016/j.molliq.2016.10.005

16. Zidane Y, Laouini SE, Bouafia A, *et al*. Green synthesis of multifunctional MgO@AgO/Ag_2O nanocomposite for photocatalytic degradation of methylene blue and toluidine blue. *Front Chem*. 2022;10:1083596.

doi: 10.3389/fchem.2022.1083596

17. Melese A, Wubet W, Abebe A, Hussen A. A comprehensive review on recent progress in synthesis methods of ZnO/CuO nanocomposites and their biological and photocatalytic applications. *Results Chem*. 2025;14:102141.

doi: 10.1016/j.rechem.2025.102141

18. Kwang Benno Park H, Kumar P, Kebaili I, *et al*. Optimization and modelling of magnesium oxide (MgO) photocatalytic degradation of binary dyes using response surface methodology. *Sci Rep.* 2024;14(1):9412.

doi: 10.1038/s41598-024-59412-6

19. Arshad A, Iqbal J, Siddiq M, *et al.* Graphene nanoplatelets induced tailoring in photocatalytic activity and antibacterial characteristics of MgO/graphene nanoplatelets nanocomposites. *J Appl Phys*. 2017;121(2):024901.

doi: 10.1063/1.4972970

20. Khan M, Tahir MN, Adil SF, *et al*. Graphene based metal and metal oxide nanocomposites: Synthesis, properties and their applications. *J Mater Chem A*. 2015;3(37):18753-18808.

doi: 10.1039/C5TA02240A

21. Kokulnathan T, Jothi AI, Chen SM, *et al*. GO-MgO nanocomposites for electrochemical detection. *J Environ Chem Eng*. 2021;9(6):106310.

doi: 10.1016/j.jece.2021.106310

22. Wang H, Li G, Fakhri A. Fabrication and structural of the Ag_2S-MgO/graphene oxide nanocomposites with high photocatalysis and antimicrobial activities. *J Photochem Photobiol B*. 2020;207:111882.

doi: 10.1016/j.jphotobiol.2020.111882

23. Kakade PM, Kachere A, Mandlik N, Rondiya SR, Jadkar S, Bhosale SV. Graphene oxide assisted synthesis of magnesium oxide nanorods. *ES Mater Manuf*. 2021;12(2):63-71.

doi: 10.30919/esmm5f1044

24. Muhaymin A, Mohamed H, Hkiri K, Safdar A, Azizi S, Maaza M. Green synthesis of magnesium oxide nanoparticles using hyphaene thebaica extract and their photocatalytic activities. *Sci Rep.* 2024;14(1):20135.

doi: 10.1038/s41598-024-70135-4

25. Rezvannasab SG, Safari N, Ghaedi AM. Synthesis and performance enhancement of GO/MgO/PEI composite for CO_2 capture: Effects of operating parameters. *J CO_2 Util*. 2025;102:103245.

doi: 10.1016/j.jcou.2025.103245

26. Bhargava R, Khan S. Superior dielectric properties and bandgap modulation in hydrothermally grown Gr/MgO

nanocomposite. *Phys Lett A*. 2019;383(14):1671-1676.

doi: 10.1016/j.physleta.2019.02.025

27. Al-Sharabi A, Sada'a KSS, Al-Osta A, Abd-Shukor R. Structure, optical properties and antimicrobial activities of MgO-Bi_2-x$CrxO_3$ nanocomposites. *Sci Rep*. 2022; 12(1):10647.

doi: 10.1038/s41598-022-14687-4

28. Barad C, Kimmel G, Opalińska A, Gierlotka S, Łojkowski W. Lattice variation as a function of concentration and grain size in MgO-NiO solid solution system. *Heliyon*. 2024;10(10):e311275.

doi: 10.1016/j.heliyon.2024.e31275

29. Khatua A, Kumari K, Khatak D, *et al*. Cerium-doped magnesium oxide nanoparticles. *J Funct Biomater*. 2023;14(2):112.

doi: 10.3390/jfb14020112

30. Yang L, Zhang L, Jiao X, Qiu Y, Xu W. The electrochemical performance of reduced graphene oxide prepared from different types of natural graphites. *RSC Adv*. 2021;11(7):4042-4052.

doi: 10.1039/D0RA09457A

31. Das A, Mandal AC, Roy S, Nambissam PM. Internal defect structure of calcium-doped magnesium oxide nanoparticles. *AIP Adv*. 2018;8(9):095206.

doi: 10.1063/1.5001105